Single- and enhanced two-beam second-harmonic generation from silicon nanocrystals by use of spatially inhomogeneous femtosecond pulses

P. Figliozzi,[1] L. Sun,[1] Y. Jiang,[1] N. Matlis,[1] B. Mattern,[1] M. C. Downer,[1]
S. P. Withrow,[2] C. W. White,[2] W. L. Mochán,[3] B. S. Mendoza[4]
[1] *FOCUS Center, University of Texas at Austin, Department of Physics, Austin, TX 78712-1081*
[2] *Oak Ridge National Laboratory, Oak Ridge, Tennessee 37831*
[3] *Centro de Ciencias Físicas, Universidad Nacional Autónoma de México, 62251 Cuernavaca, Morelos, México and*
[4] *Centro de Investigaciones en Optica, León, Guanajuato, México*

Optical second harmonic generation (SHG) is used as a noninvasive probe of the interfaces of Si nanocrystals (NCs) embedded uniformly in an SiO_2 matrix. Measurements of the generated SH mode verify that the second-harmonic polarization has a nonlocal dipole form proportional to $(\vec{E}\cdot\nabla)\vec{E}$ that depends on inhomogeneities in the incident field $\vec{E}$, as proposed in recent models based on a locally noncentrosymmetric dipolar response averaged over the spherical NC interfaces. A two-beam SHG geometry is found to enhance this polarization greatly compared to single-beam SHG, yielding strong signals useful for scanning, spectroscopy and real-time monitoring. This configuration provides a general strategy for enhancing the second-order nonlinear response of centrosymmetric samples, as demonstrated here for both Si nano-composites and their glass substrates.

PACS numbers: 42.65.-Ky, 78.40.Fy, 78.68.+m

The unique electronic structure of Si nanocrystals (NCs) embedded in SiO_2 is enabling new light-emitting[1,2] and flash-memory[3] devices that can be fabricated with standard methods of microelectronics technology. Electronic states at the *interfaces* of the Si NCs with the SiO_2 matrix play a key role in the physics of such devices. For example, Wolkin *et al.* proposed that Si=O double bonds become stable and luminesce at the interfaces of Si NCs of a few nm diameter.[4] Oxygen vacancies give rise to additional interface states[5] that can trap photo-excited charge, quench luminescence, and mediate storage and release of charge. However, the microscopic nature and energy spectrum of these interface states is still under debate,[4,5] in part because of the lack of effective experimental probes of the NC/SiO_2 interface.

Optical second harmonic generation (SHG) can provide such a probe. In a recent work,[6] we observed weak SHG from Si NCs embedded in SiO_2 and demonstrated its sensitivity to chemical modification of the sharply curved Si NC/SiO_2 interfaces. Thus evidently the interface sensitivity of SHG, widely exploited in probing *planar* Si/SiO_2 interfaces,[7] persists even for macroscopically centrosymmetric composites of spherical Si NCs. The mechanism of SHG, however, remained unclear. Recent phenomenological models of SHG from individual spherical particles of centrosymmetric material,[8,9] and from nano-composites,[10] have shown that the lowest order contributions to the SH polarization density $\vec{P}^{(2)}$ are[11]

$$\vec{P}^{(2)}_{SHG} = n_{NC}\vec{p}^{(2)} - \frac{1}{6}\nabla\cdot n_{NC}\overleftrightarrow{Q}^{(2)}. \qquad (1)$$

The first term represents the contribution from the SH dipole moments $\vec{p}^{(2)}$ of individual nanoparticles of uniform density n_{NC}. $\vec{p}^{(2)}$ has a nonlocal form, with its radiative part proportional to $(\vec{E}\cdot\nabla)\vec{E}$, that results from spherically averaging the locally noncentrosymmetric dipole polarization $\overleftrightarrow{\chi}^{(2)}_s : \vec{E}\vec{E}$ of the Si/SiO_2 interface, with additional contributions from the bulk Si. Here $\overleftrightarrow{\chi}^{(2)}_s$ is the second-order nonlinear susceptibility of the interface and $\vec{E}$ is the incident field. The second term describes additional contributions from the SH quadrupole moment $\overleftrightarrow{Q}^{(2)}$, which enhance SHG in regions of local gradients ∇n_{NC} in NC density.[6] In this Letter, we demonstrate a clear experimental signature of the $(\vec{E}\cdot\nabla)\vec{E}$ form of $n_{NC}\vec{p}^{(2)}$ in the transverse mode structure of the SH signal generated by a single incident beam from a locally uniform Si NC composite. We then exploit this form of $\vec{P}^{(2)}_{SHG}$ to generate unprecedented SH intensity from the NCs by shifting to a configuration with two noncollinear, orthogonally-polarized fundamental beams. Previously, two-beam SHG has been applied to *non*-centrosymmetric samples to determine precisely the tensor components of the dipole-*allowed* $\overleftrightarrow{\chi}^{(2)}$.[12] Here, we demonstrate, for the first time to our knowledge, that two-beam SHG provides a general strategy for enhancing the second-order nonlinear response of centrosymmetric materials, including the Si nano-composite as well as its glass substrate.

Samples were prepared by sequentially implanting Si ions of different energies into 0.9 mm thick silica substrates to a depth of 1 μm, then annealing for 1 h at 1100 ^{o}C in Ar to precipitate formation of NCs of uniform density $n_{NC} = 7, 3$ and 1.5×10^{18} cm^{-3}, and average diameters $\langle d_{NC}\rangle = 3$, 5 and 8 nm, respectively.[13,14] No NCs were implanted in an outer 1 mm wide margin of each substrate, which therefore served as a control sample to monitor SHG from the unimplanted glass. We measured single-beam SHG in transmission using linearly polarized pulses of duration $\tau_p = 200$ fs, energy $\mathcal{E} = 0.3\mu$J at repetition rate $f_{rep} = 250$ kHz from a regeneratively amplified Ti:S laser. Pulses were focused at normal incidence to a spot radius $w_0 \approx 10\mu$m onto the sample with TEM_{00} mode structure (see Fig. 1a, top). The unimplanted glass produced no detectable SHG. However, the

signal climbed immediately to ~ 100 SH photons/s (*i.e.* 4×10^{-4} SH photons/pulse) as the laser spot scanned into the implant (Fig. 1b), proving that the NCs produced the signal. We imaged the SH beam generated by a uniform region of Si NCs ($\nabla n_{NC} = 0$) from the sample onto a photon-counting charge-coupled device (CCD) (Fig. 1a). The image shows that the NCs emitted SH in a double-lobed TEM_{01} mode (Fig. 1a, bottom left), with no SHG in the exact forward direction. With a single-beam, the only contribution to ∇E that radiates in the near-forward direction is the transverse gradients of the incident TEM_{00} mode, which point radially outward from its center. Thus for incident linear polarization $(\vec{E} \cdot \nabla)\vec{E}$ has the spatial structure shown in Fig. 1a (bottom right), which is in excellent agreement with the observed mode structure. This mode structure strikingly confirms the predicted[9,10] $(\vec{E} \cdot \nabla)\vec{E}$ form of $\vec{P}^{(2)}_{SHG}$.

The intensity scaling of the SHG signal also confirms the $(\vec{E} \cdot \nabla)\vec{E}$ mechanism, for which SH count rate (SH photons/s) scales as $f_{rep}\mathcal{E}^2/(\pi w_0^2)^2\tau_p$, in view of the finite waist w_0 of the TEM_{00} Gaussian beam. In principle, higher $\mathcal{E}$ or smaller w_0 increases signal. However, incident fluence $\mathcal{E}/\pi w_0^2$ was limited to $\lesssim 0.1$ J/cm^2 by the onset of sample damage. Instead, we repeated the single-beam measurements using 80 fs, 50 μJ pulses at $f_{rep} = 1$ kHz from a more powerful Ti:S amplifier. To avoid damage, w_0 was increased to 125μm. Ironically the more powerful pulses yielded $\sim 100\times$ *fewer* counts/s, in agreement with the above scaling law. Had $\vec{P}^{(2)}_{SHG}$ been dipolar, the SHG signal would have scaled as $f_{rep}\mathcal{E}^2/\pi w_0^2\tau_p$, yielding $\sim 10\times$ *stronger* signal, contrary to observation.

A consequence of the $(\vec{E}\cdot\nabla)\vec{E}$ form of $\vec{P}^{(2)}_{SHG}$ is that the SH response can be enhanced significantly in a two-beam SHG geometry. To demonstrate this, we split the 50μJ pulses equally and recombined the two pulses with spot size $w_0 = 125\mu$m (thus maintaining sub-damage fluence) as illustrated in Fig. 2. The sample surface lies in the xy plane, $\vec{E}_1$ is normally incident, while $\vec{E}_2$ is obliquely incident with p-polarization. In this geometry

$$\vec{P}^{(2)}_{SHG} = in_{NC}[(\vec{E}_1 \cdot \vec{k}_2)\vec{E}_2 + (\vec{E}_2 \cdot \vec{k}_1)\vec{E}_1]e^{i(\vec{k}_1+\vec{k}_2)\cdot\vec{r}} \quad (2)$$

for $\nabla n_{NC} = 0$, where $\vec{E}_{1,2}$ and $\vec{k}_{1,2}$ are the incident fields and wave-vectors inside the sample, and we have used the plane wave approximation, thus neglecting the weak single beam SH polarizations. When $\vec{E}_1$ is polarized along $\hat{y}$, $\vec{E}_1 \cdot \vec{k}_2 = 0$, but $(\vec{E}_2 \cdot \vec{k}_1)\vec{E}_1 = ikE_1E_2 \sin\alpha\hat{y}$ contributes a strong forward-radiating polarization, where α is the angle between $\vec{k}_1$ and $\vec{k}_2$ inside the sample. Now a wavelength-scale gradient $\propto 1/\lambda$ replaces the spot-size-scale transverse gradient $\propto 1/w_0$ in single-beam SHG, resulting in a much stronger signal that scales as $\sin^2\alpha\mathcal{E}_1\mathcal{E}_2 f_{rep}/\lambda^2\pi w_0^2\tau_p$ and propagates along $\vec{k}_1 + \vec{k}_2$. We observed two-beam SHG to be stronger by orders of magnitude (*e.g.* $\sim 10^4$ counts/s or 10 counts/pulse for $\alpha = 20^0$) than single-beam SHG. In fact, photon counting was no longer required. By contrast, when $\vec{E}_1$ and $\vec{E}_2$ lie in the xz plane, the bracketed term in Eq (2) becomes $-iE_1E_2\frac{\sin^2\alpha}{1+\cos\alpha}(\vec{k}_1 + \vec{k}_2)$, which points along the propagation direction, and thus does not radiate. As a result, we observe a signal comparable to single-beam SHG. As we varied the angle θ between the $\vec{E}_1$ and the xy projection of $\vec{E}_2$, the SHG signal, now detected by a conventional analog PMT, varied as $\sin^2\theta$, as shown in Fig. 2. SHG is maximized for $\vec{E}_1 \perp \vec{E}_2$. Essentially identical results were obtained when $\vec{E}_2$ was rotated with fixed $\vec{E}_1$, the maximum again occurring for $\vec{E}_1 \perp \vec{E}_2$. The maximum observed for $\vec{E}_1 \| \hat{x}$ and $\vec{E}_2 \| \hat{y}$ is significant because two-beam SHG from the isotropic glass *surface*

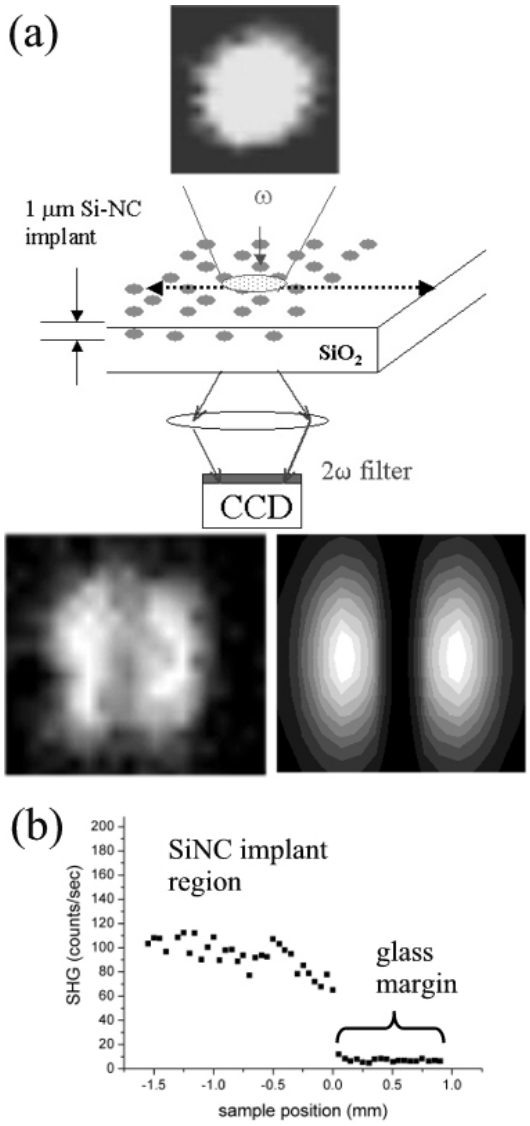

FIG. 1: a) Experimental set-up for single-beam SHG, showing incident TEM_{00} fundamental mode (top), and the measured (bottom left) and calculated (bottom right) TEM_{01} mode of the imaged SH radiation. b) Scan of integrated SHG signal across the boundary between Si NC implant and unimplanted glass rim at edge of sample.

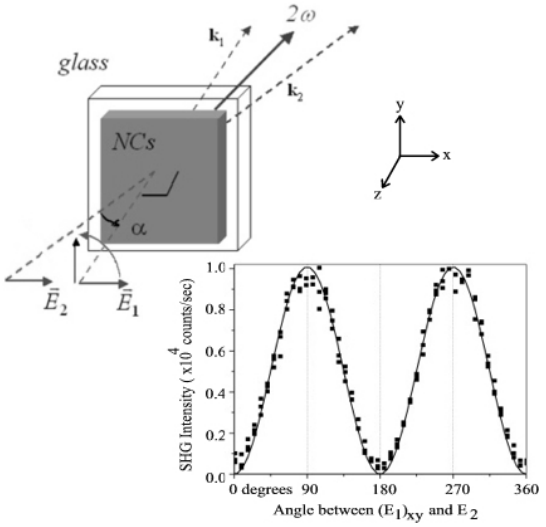

FIG. 2: Schematic of two-beam SHG configuration using incident fields $\vec{E}_1$ and $\vec{E}_2$ with wave vectors $\vec{k}_1$ and $\vec{k}_2$ intersecting at angle α inside the sample. Lower right: dependence of two-beam SHG on the angle between $\vec{E}_1$ and the projection of $\vec{E}_2$ in the xy plane, for the sample with $\langle d_{NC}\rangle = 5$ nm.

is forbidden. Significant glass surface contributions to the enhanced two-beam SHG can thus be ruled out. We confirmed that two-beam SHG contained only frequencies within the doubled fundamental spectrum, and depended on temporal overlap of the incident pulses.

A complication arose, however, because the two-beam SHG geometry with $\vec{E}_1 \perp \vec{E}_2$ also enhanced the signal from the isotropic glass substrate, whose second-order transverse polarization is also $\propto (\vec{E}\cdot\nabla)\vec{E}$, because of its bulk isotropy. This is evident from the SHG scans across the glass/NC boundary in Fig. 3a, which now show comparable signal from the unimplanted glass rim and the NC-implanted glass. Consequently, both the glass substrate and the 1-μm thick Si NC implant contributed to the enhanced SHG shown in Fig. 2. Evidently two-beam SHG with $\vec{E}_1 \perp \vec{E}_2$ can be used quite generally for enhancing the SH response of centrosymmetric materials such as glass, which possess a bulk quadrupolar response of the same macroscopic form as the spherically-averaged interface response of a nano-composite. The reason for the reduced contrast between NC- and glass-generated SHG in the two-beam, as compared to single-beam, experiments remains unsettled. Naively we expect that both signals, being $\propto \vec{E}\cdot\nabla\vec{E}$, should be enhanced by the same factor $\sim \sin^2\alpha w_0^2/\lambda^2$. However, single-beam SHG may be dominated by NCs close to the top and bottom surfaces of the implanted region, where they are influenced by additional inhomogeneities of their image field[9] which are not enhanced in the two-beam geometry. Further work is under way to elucidate this point.

Fortunately, the two enhanced contributions can be discriminated completely with additional independent measurements, as illustrated in Fig. 3. Fig. 3a contrasts two SHG scans in which an NC layer ($\langle d\rangle = 5$ nm) is either on the beam exit (open triangles) or entrance (filled squares) side of the substrate. SHG from the implanted region is stronger (weaker) than from the unimplanted glass with the NCs on the exit (entrance) side. The asymmetry is more pronounced for 8 nm, less for 3 nm NCs (not shown). This asymmetry arises because, with NCs at the exit, they absorb $\sim 2/3$ of the SHG from the glass.[6] They then generate additional signal, resulting in stronger SHG than from unimplanted glass. The weaker SHG observed with NCs at the entrance proves that the SH fields $E_g^{2\omega}$ and $E_{NC}^{2\omega}$ from glass and NC layer, respectively, interfere destructively.

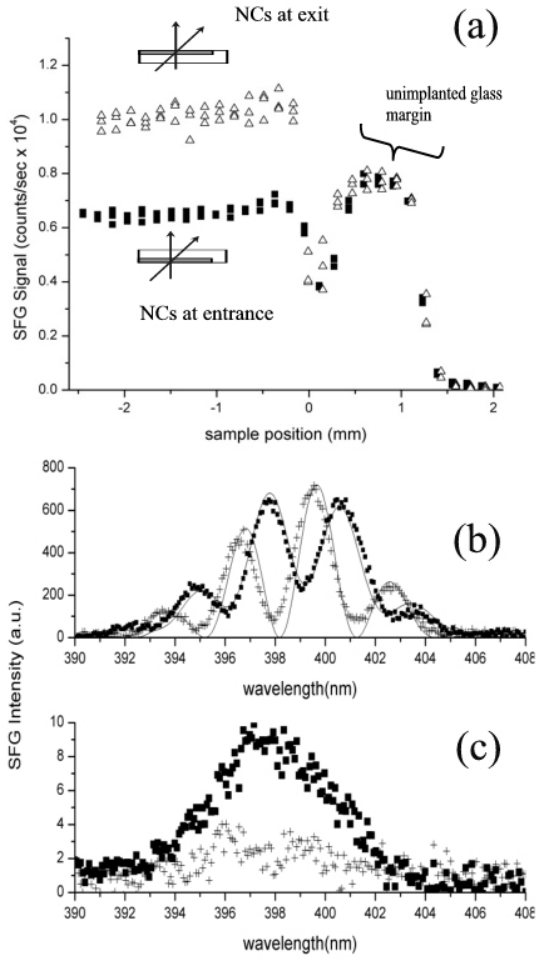

FIG. 3: (a) Scan of two-beam SHG across glass/NC boundary with NC layer ($\langle d_{NC}\rangle = 5$ nm) at entrance (filled squares) or exit (triangles) side of sample, with orthogonally-polarized incident fields. (b) Spectrally dispersed two-beam SHG from unimplanted glass (crosses) and NC implant (filled squares) of same sample with NCs at exit, showing Maker fringes caused by frequency-dependent phase mismatch in glass substrate. (c) Same as (b) but for parallel polarization of incident fields.

To quantify the phase relationship between $E_g^{2\omega}$ and $E_{NC}^{2\omega}$, we spectrally dispersed SH light generated in

the unimplanted and NC-implanted regions in a spectrometer, as shown in Fig. 3b. The signal from the glass rim (crosses) shows several Maker fringes[15] within the SH bandwidth. These result from frequency-dependent phase mismatch within the glass substrate, which is $\sim 100\pi/\Delta k_g$ thick, where $\Delta k_g = |\vec{k}_1 + \vec{k}_2 - \vec{k}_3|$ is the phase mismatch inside the sample. The curve through the crosses represents the square modulus of the calculated phase-mismatched SH field $E_g^{2\omega} = \Gamma_g(\Delta k)^{-1}E^2(\omega)(e^{i\Delta k_g L_g} - 1)$, where we used measured values of spectral intensity profile $|E(\omega)|^2$, refractive indices $n_g(\omega)$ and $n_g(2\omega)$ to calculate Δk, and the effective glass thickness L_g along $\vec{k}_1 + \vec{k}_2$. Excellent agreement is obtained despite using no fitting parameters other than an overall real scaling factor Γ_g. No spatial variations in this signal were observed within the unimplanted glass, indicating that its thickness was uniform. The field $E_g(\omega)$ is thus well characterized. Significantly, the signal $|E_g^{2\omega}|^2$ drops to approximately zero at 395, 398, 401 and 404 nm. At these 4 wavelengths, the non-zero SHG signal from the NC-implanted region, shown by filled squares in Fig. 3b, can be regarded as pure NC signal. At intervening frequencies, the $E_g(2\omega)$ acts as a local oscillator that interferes with $E_{NC}^{2\omega}$. Since the NC layer is much thinner than $\pi/\Delta k_{NC} \approx 13\mu m$,[6] phase mismatch is small and does not produce Maker fringes in $E_{NC}^{2\omega}$. It can be written $i\Gamma_{NC}(i\Delta k + \alpha_{NC}^{2\omega})^{-1}(e^{i\Delta k L_{NC}} - e^{-\alpha L_{NC}})E^2(\omega)$,[17] where $\alpha_{NC}^{2\omega}$ and L_{NC} are the linear absorption coefficient and thickness, respectively, of the NC layer, and we take the nonlinear coefficient Γ_{NC} as a complex, frequency-independent constant. The curve through the filled squares represents a fit to $|E_{NC}^{2\omega} + E_g^{2\omega}|^2$, where $E_g^{2\omega} = \Gamma_g(\Delta k)^{-1}e^{(-\alpha_{NC}^{2\omega} + i\Delta k)L_{NC}}(e^{i\Delta k_g L_g} - 1)E^2(\omega)$ when its propagation through the NC layer is taken into account.[17] For the fitted value $\Gamma_{NC}/\Gamma_g = P_1 e^{iP_2}$ relative to Γ_g we obtain $P_1 = 1.35 \pm .01$ and $P_2 = 0.39\pi \pm .002\pi$. The presence of a significant positive phase shift of Γ_{NC} relative to Γ_g suggests that 2ω lies just below a resonance of the Si NCs. Indeed a modified E_1 resonance at $\hbar\omega = 3.32$ eV, near the SH photon energy, has been observed in $\langle d \rangle = 5$ nm Si NCs.[16] Thus we have discriminated Γ_{NC} completely from Γ_g, while retaining the strong signal enhancement of the $\vec{E}_1 \perp \vec{E}_2$ configuration.

For contrast, Figure 3c shows the much weaker spectrally-resolved SFG signals from the unimplanted glass (crosses) and NC-implanted region (filled squares) in the $\vec{E}_1 \| \vec{E}_2$ configuration. As for single-beam SHG, the glass yields negligible signal, so the high contrast between the NC implant and glass is recovered, at the cost of smaller signal. The absence of Maker fringes in the two-beam SHG from the NC implant is consistent with the absence of a glass substrate contribution.

In conclusion, we have experimentally verified that SHG from a uniform composite of spherical Si NCs is radiated by a nonlinear polarization of nonlocal dipolar form proportional to $(\vec{E} \cdot \nabla)\vec{E}$. We showed that SH responses of this form are greatly enhanced in a noncollinear two-beam SHG configuration, whether they originate microscopically from spherical interfaces (as in the nano-composite) or from a bulk quadrupolar response (as in the glass substrate). Competing signals from NCs and substrate were discriminated straightforwardly, and detectable without photon counting. We are currently exploiting this configuration for spectroscopic SHG of the NC-oxide interfaces, by using a widely tunable pulse from an optical parametric amplifier. This configuration should be widely applicable for noninvasive spectroscopy of the electronic structure of buried nano-interfaces.

This work was supported by NSF grants DMR-0207295 and PHY-0114336 and by Robert Welch Foundation grant F-1038. Oak Ridge Laboratory is managed by UT-Batelle, LLC under U.S. Dept. of Energy Contract DE-AC05-00OR22725.

[1] L. Pavesi, L. Dal Negro, C. Mazzoleni, G. Franzo, and F. Priolo, Nature **408**, 440 (2000).
[2] W. L. Ng, M. A. Lourenco, R. M. Gwilliam, S. Ledain, G. Shao and K. P. Homewood, Nature (London) **410**, 192 (2001).
[3] S. Tiwari, F. Rana, H. Hanafi, A. Hartstein, E. F. Crabbe, and K. Chan, Appl. Phys. Lett. **68**, 1377 (1996).
[4] M. V. Wolkin, J. Jorne, P. M. Fauchet, G. Allan and C. Delerue, Phys. Rev. Lett. **82**, 197 (1999).
[5] E. Degoli and S. Ossicini, Surf. Sci. **470**, 32 (2000).
[6] Y. Jiang, P. T. Wilson, M. C. Downer, C. W. White and S. P. Withrow, Appl. Phys. Lett. **78**, 766 (2001).
[7] G. Lüpke, Surf. Sci. Rep. **35**, 75 (1999); M. C. Downer, B. S. Mendoza and V. I. Gavrilenko, Surf. Interface Anal. **31**, 966 (2001).
[8] J. Dadap, J. Shan, K. Eisenthal and T. F. Heinz, Phys. Rev. Lett. **83**, 4045 (1999).
[9] V. Brudny, B. Mendoza and W. Mochan, Phys. Rev. B **62**, 11152 (2000).
[10] W. L. Mochan, J. A. Maytorena, B. S. Mendoza and V. Brudny, Phys. Rev. B **68**, 85318 (2003).
[11] G. Russakoff, Am. J. Phys. **38**, 1188 (1970).
[12] S. Cattaneo and M. Kauranen, Opt. Lett. **28**, 1445 (2003).
[13] C. W. White, S. P. Withrow, A. Meldrum, J. D. Budai, D.M. Hembree, J. G. Zhu, D. O. Henderson, and S. Prawer, Mat. Res. Soc. Symp. Proc. **507**, 249 (1998).
[14] S. P. Withrow, C. W. White, A. Meldrum, J. D. Budai, J. D. M. Hembree, and J. C. Barbour, J. Appl. Phys. **86**, 396 (1999).
[15] P. D. Maker, R. W. Terhune, M. Nisenoff and C. M. Savage, Phys. Rev. Lett. **8**, 21 (1962).
[16] Y. Jiang, L. Sun and M. C. Downer, Appl. Phys. Lett. **81**, 3034 (2002).
[17] Y. R. Shen, *The Principles of Nonlinear Optics* (New York, Wiley & Sons, 1984), section 6.6.